

Structure change of MgSiO₃, MgGeO₃, and MgTiO₃ ilmenites under compression

T. YAMANAKA,* Y. KOMATSU, M. SUGAHARA, AND T. NAGAI

Department of Earth and Space Science, Graduate School of Science, Osaka University, 1-1 Machikaneyama, Toyonaka, Osaka 560-0043, Japan

ABSTRACT

Compression mechanisms of A²⁺B⁴⁺O₃ ilmenites with compositions MgSiO₃ (stable at high pressures), MgGeO₃ (stable at moderate pressures), and MgTiO₃ (stable at ambient pressure) were investigated at high pressure by single-crystal structure analysis, using both synchrotron radiation and an MoK α rotating-anode X-ray generator. The distortions of AO₆ (A: Mg) and BO₆ (B: Si, Ge, Ti) octahedra under pressure were parameterized by bond length, shared-face area, site-volume ratio, and A²⁺-B⁴⁺ interatomic distance across the shared edges and shared face. The AO₆ octahedral volume is much more compressive than the BO₆ octahedral volume. Of the three samples, both the AO₆ and BO₆ octahedra are most rigid in MgSiO₃. The A²⁺-B⁴⁺ interatomic distance becomes more shortened with increasing pressure than do the A²⁺-A²⁺ and B⁴⁺-B⁴⁺ distances. The compression of Mg-Si is more remarkable than that of Mg-Ge and Mg-Ti. The A-B interatomic distance along **c** is more compressed with increasing pressure than A-A and B-B along **a**. The short A-B distance across the shared face becomes more shortened than the A-A and B-B distances across the shared edge. The cation position moves in the direction of **c** with pressure and tends to approach the center of the AO₆ and BO₃ octahedra with increasing pressure. The regularity of the octahedra is enhanced at higher pressure. Both quadratic elongation and bond angle variance verify the reduction of the deformation of AO₆ and BO₆ octahedra with pressure.

INTRODUCTION

Ilmenite and its related compounds have attracted material scientists and crystal chemists because of their practical applications. A²⁺B⁴⁺O₃ ilmenite compounds are composed of a relatively large A cation (A: Mg, Fe, Mn, Co, Zn) and a small B cation (B: Si, Ge, Sn, Ti). However, compounds with a large ion radii ratio R_A/R_B , such as CaTiO₃ and BaTiO₃, do not form ilmenite structures but have the perovskite structure at ambient pressure. Many ilmenites transform to perovskite at high pressure because oxygen is more compressible than the cations and thus the R_A-R_0/R_B-R_0 ratio increases with pressure. The *P-T* regions where these ilmenites are stable vary systematically with the cation radius ratios.

The MgSiO₃ ilmenite phase is one of the high-pressure polymorphs of orthoenstatite. It has been much studied because it is one of the essential phases in the upper mantle, in spite of the fact that its stable region of pressure and temperature is relatively limited, being 20–24 GPa and 1100–2000 °C (Ito and Yamada 1982; Ito and Navrotsky 1985; Sawamoto 1987). (Mg,Fe)SiO₃ ilmenite was found in the shock vein of meteorite and was named akimotoite (Tomioka and Fujino 1997). MgTiO₃ geikielite is found as an accessory mineral in many igneous and metamorphic rocks (Deer and Zussman 1962) and can be

synthesized at ambient pressure.

The crystal structure of MgSiO₃ ilmenite was analyzed by single crystal X-ray diffraction study at ambient conditions (Horiuchi et al. 1982) and by Rietveld profile fitting under high pressure (Reynard and Rubie 1996). Molecular dynamics simulation of MgSiO₃ ilmenite has been carried out (Matsui et al. 1987; Karki et al. 2000) and a Raman spectroscopic study has been made (Reynard et al. 1996). MgGeO₃ shows the same polymorphic transitions as MgSiO₃, but their transition pressures are much lower than the corresponding pressures of the MgSiO₃ polymorphs (Ross and Navrotsky 1988).

The structures of corundum ($R\bar{3}c$), ilmenite ($R\bar{3}$), and LiNbO₃ ($R3$) are crystallographically closely related and are characterized by different ordering of A and B cations. It has been reported that some LiNbO₃-type structures were found as metastable phases on release of pressure from perovskite stable region. However, there is no clear evidence that the LiNbO₃-type phases are really metastable. Under decompression after forming perovskite, MgGeO₃, MgTiO₃, MnTiO₃, MnSnO₃, and FeTiO₃ ilmenites did not show a reversible transformation to ilmenite but they transformed to the LiNbO₃ or disordered ilmenite structure (Ko and Prewitt 1988; Ross and Leinenweber 1990; Ross et al. 1988, 1989; Lipton et al. 1997, 1999; Leinenweber et al. 1991, 1994). These transformations are monotropic. LiNbO₃ undergoes a transformation to perovskite under high pressure and the transition is enantiotropic and reversible (Mukaida et al. 2003). No

* E-mail: yamanaka@hpc.cmc.osaka-u.ac.jp

satisfactory crystal chemical explanation has been given for the monotropic transformation of ilmenite under decompression. No structure refinements have been made to prove the capability of cation disorder. The ilmenite structure has unique face-shared and edge-shared configurations of AO₆ and BO₆ octahedra. Cation-cation interactions in the structure have a significant meaning not only for the degree of disorder but also for physical properties such as ferroelectricity and magnetism. The present in situ high-pressure investigations of synthetic ilmenite-type MgXO₃ phases discuss the pressure-induced stereochemical changes and crystal chemical comparisons between the behaviors of the individual structures.

Single crystal synthesis

A sintered sample of MgSiO₃ enstatite was used as the starting material and kept at 1700 °C and 23 GPa for 30 min in the 6–8 type multi-anvil high-pressure apparatus at Misasa. Prismatic transparent single crystals of MgSiO₃ ilmenite of several hundred micrometers long were synthesized. The single crystals of MgGeO₃ ilmenite were grown at 6 GPa and 900 °C for 12 hours using a cubic multi-anvil press. The starting mixture of MgO and GeO₂ was kept in a gold tube to prevent sample reduction. H₂O was used as a flux to synthesize large grains and transparent crystals of MgGeO₃ ilmenite 200 μm long. MgTiO₃ ilmenite was prepared by solid-solid reaction of MgO and TiO₂ (rutile) at ambient pressure. The starting material was heated in a Pt crucible at 1550 °C for 80 h and the single crystals about 350 μm in length were synthesized.

Homogeneity and chemical impurities in the grown crystals were examined by EPMA. The stoichiometry of the samples was also confirmed. An optical microscope and X-ray diffraction using an imaging plate were used to test the crystallinity. Approximately cube-shaped crystals about 60 μm in edge length were selected for the high-pressure X-ray diffraction experiments.

High-pressure diffraction

Single-crystal structure refinements under high pressure were carried out using a diamond anvil cell (DAC). The in situ diffraction intensity measurements encountered many difficulties, including hydrostaticity, blind region due to the limited aperture angle of the pressure cell, X-ray absorption from the window, and limitations of sample size. Our DAC with a large diamond backing plate greatly improves the accuracy of the structure analysis (Yamanaka et al. 2001). Diamond (100) plate windows of 6 × 6 mm wide and 2 mm thick have the following advantages: lower X-ray mass absorption, much higher-pressure generation over 50 GPa, no powder rings from the window, and wider observable 2θ angle. These advantages have been previously employed to determine the precise charge-density distribution of stishovite at 30 GPa (Yamanaka et al. 2002).

A single crystal about 40 × 40 μm wide and 20 μm thick was placed in the preintended gasket hole of 200 μm in diameter. Ruby chips for pressure marker and pressure transmitting media were also kept in the hole. The medium was an alcohol mixture with methanol:ethanol:H₂O = 16:3:1. Hydrostatic conditions could be guaranteed for pressures up to 15 GPa.

The intensity measurements were carried out using synchrotron radiation (SR) at BL10A in the Photon Factory at KEK and with an MoKα rotating anode X-ray generator. The SR incident beam was monochromated by Si (111) double crystals. The beam of λ = 0.6965 Å (E = 17.80 eV) was focused on the DAC by a mirror and a collimator guide pipe for reducing the background intensity. A divergent slit 100 μm in diameter and a receiving slit 1.5 mm wide were applied in consideration of the size of the gasket hole and the sample.

A HUBER four-circle diffractometer with a scintillation counter was used for the diffraction intensity measurement at KEK. The UB matrix was determined on the basis of reflections in the range 20° < 2θ < 30°. Intensity measurements were made with φ-fixed and ω-scanning mode, a scan speed of 1 °/min, a scan width of

about 0.8–1.0° in ω-scan, and a step interval of 0.01 °/step. Intensity corrections for polarization of the SR and a Lorentz factor for the scanning mode were taken into account and the following equation was applied:

$$1/L_p = \sin 2\theta / (\cos^2 2\theta + \cos^2 2\theta_M) \quad (1)$$

The intensities were corrected for the absorption effects ($\mu_r = 0.062\text{--}0.9$) from samples together with the diamond window plates and anvils. Reflection intensities within 2θ < 60° were observed between 390 and 480 for each sample. Crystallographically independent reflections with $|F_o| > 3\sigma|F_c|$ after averaging the equivalent reflections were used for the least-squares refinements. The number of observed reflections was more than that obtained with the laboratory source.

In the laboratory high-pressure diffraction studies used MoKα radiation (λ = 0.71069 Å) monochromated by pyrolytic graphite and emitted from the rotating-anode generator operated at 55 kV and 150 mA. φ-fixed and ω-scanning modes were applied with scan widths of about 1.5° in 2θ and scan speeds of 1 °/min. The experimental conditions are presented in Table 1.

The structure refinements were carried out using the full-matrix least-squares program RADY written by Sasaki (1987). The atomic scattering factor *f*_i for the fully ionized *i*-atom was taken from the *International Tables for X-ray Crystallography* (1974). The atomic coordinates, site occupancy parameter, isotropic temperature factors, and isotropic extinction parameter were chosen as the variable parameters. The refined structure parameters at each pressure are presented in Table 2. The following reliability factors (*R* and *wR*) of the least-squares refinement are also presented in the table:

$$R = \frac{\sum(|F_o| - |F_c|)}{\sum|F_o|}, \quad wR = \left[\frac{\sum w(|F_o|^2 - |F_c|^2)^2}{\sum w|F_o|^2} \right]^{1/2} \quad (2)$$

where $w = 1/\sigma^2(|F_o|)$ and σ is the standard deviation of the observed intensity.

Compression of unit-cell volume

The lattice parameters were determined by the least-squares method based on the *d* values of 15–25 reflections in the range 20° < 2θ < 30°. The lattice parameters, *c/a* axial ratios, and unit-cell volumes of MgSiO₃, MgGeO₃, and MgTiO₃ are presented in Table 1. The changes in *c/a* with pressure indicate that the *c* lattice parameter is more compressive than *a*. The lattice parameters of MgSiO₃ were less compressive compared with those of MgGeO₃ and MgTiO₃. This is consistent with the fact that MgSiO₃ ilmenite is stable over 20 GPa, whereas MgGeO₃ and MgTiO₃ are stable at moderate pressure and ambient pressure,

TABLE 1. Pressure dependence of lattice constants and unit cell volume

MgSiO₃					
Press (GPa)	0.0001	3.5	5.7	7.8	
diffractometer	AFC5	SR	SR	SR	
<i>a</i> (Å)	4.729(1)	4.707(3)	4.697(2)	4.688(1)	
<i>c</i> (Å)	13.559(2)	13.474(9)	13.408(9)	13.354(8)	
<i>c/a</i>	2.867	2.863	2.854	2.849	
<i>V</i> (Å ³)	262.6(1)	258.5(3)	256.1(2)	254.1(2)	
MgGeO₃					
Press (GPa)	0.0001	1.8	4.7	8.1	9.3
diffractometer	AFC5	AFC6	AFC6	AFC6	SR
<i>a</i> (Å)	4.9375(8)	4.923(2)	4.907(2)	4.880(3)	4.871(1)
<i>c</i> (Å)	13.743(1)	13.687(7)	13.605(5)	13.502(6)	13.458(2)
<i>c/a</i>	2.783	2.780	2.773	2.767	2.763
<i>V</i> (Å ³)	290.1(2)	287.2(2)	283.6(2)	278.5(2)	276.5(2)
MgTiO₃					
Press (GPa)	0.0001	3.1	5.8	8.1	
diffractometer	AFC5	AFC6	AFC6	AFC6	
<i>a</i> (Å)	5.0540(9)	5.028(2)	5.006(2)	4.992(2)	
<i>c</i> (Å)	13.898(1)	13.79(6)	13.689(6)	13.609(7)	
<i>c/a</i>	2.750	2.743	2.735	2.726	
<i>V</i> (Å ³)	307.4(1)	301.8(3)	297.1(3)	293.7(5)	

Notes: The numbers in parentheses denote errors in the last decimal place. AFC5 and SR indicate data taken using a MoKα rotating-anode X-ray generator and synchrotron radiation at KEK Tsukuba, respectively.

TABLE 2. Result of structure refinements

MgSiO ₃					
Press(GPa)	0.0001	3.5	5.7	7.8	
diffractometer	AFC5	SR	SR	SR	
No. of ref. obs	927	356	337	324	
No of ref. used	523	292	265	260	
R(%)	2.3	3.9	3.9	4.1	
wR(%)	2.5	3.5	3.2	3.1	
Mg z	0.36029(7)	0.3592(1)	0.3582(5)	0.3577(5)	
B _{eq}	0.51(1)	0.65(8)	0.63(10)	0.41(11)	
Si z	0.15773(5)	0.1574(1)	0.1575(3)	0.1572(4)	
B _{eq}	0.30(1)	0.49(6)	0.39(8)	0.28(10)	
O x	0.3230(2)	0.3232(7)	0.3225(14)	0.3261(16)	
y	0.0366(2)	0.0365(7)	0.0365(15)	0.0384(17)	
z	0.23956(7)	0.2401(1)	0.2403(5)	0.2408(5)	
B _{eq}	0.39(1)	0.49(6)	0.45(10)	0.47(12)	
MgGeO ₃					
Press(GPa)	0.0001	1.8	4.7	8.1	9.3
diffractometer	AFC5	AFC6	AFC6	AFC6	SR
No of ref. obs	1010	231	242	233	347
No of ref. used	741	176	143	124	283
R(%)	2.9	3.5	4.6	4.7	3.4
wR(%)	2.8	4.2	4.5	4.0	2.7
Mg z	0.3590(2)	0.3592(4)	0.3589(7)	0.3587(11)	0.3581(5)
B _{eq}	0.56(4)	0.42(5)	0.35(8)	0.37(8)	0.33(4)
Ti z	0.15363(6)	0.1534(1)	0.1536(2)	0.1535(3)	0.1528(1)
B _{eq}	0.36(1)	0.26(2)	0.18(4)	0.19(4)	0.29(2)
O x	0.3170(8)	0.3169(8)	0.3164(16)	0.3183(16)	0.3157(7)
y	0.0273(8)	0.0268(8)	0.0261(16)	0.0262(17)	0.0244(7)
z	0.2436(2)	0.2439(5)	0.2440(8)	0.2445(12)	0.2447(6)
B _{eq}	0.53(4)	0.35(5)	0.24(8)	0.19(8)	0.24(5)
MgTiO ₃					
Press(GPa)	0.0001	3.1	5.8	8.1	
diffractometer	AFC5	AFC6	AFC6	AFC6	
No of ref. obs	1150	283	271	252	
No of ref. used	817		126	103	158
R(%)	2.4	4.6	4.7	3.2	
wR(%)	2.1	4.4	4.6	4.0	
Mg z	0.35563(6)	0.3560(9)	0.3559(9)	0.3560(9)	
B _{eq}	0.54(1)	0.58(8)	0.48(8)	0.50(8)	
Ti z	0.14496(2)	0.1447(4)	0.1453(4)	0.1446(4)	
B _{eq}	0.41(1)	0.31(4)	0.25(5)	0.02(5)	
O x	0.3159(1)	0.3167(15)	0.3152(14)	0.3143(14)	
y	0.0218(1)	0.0222(16)	0.0222(15)	0.0199(14)	
z	0.24641(5)	0.2473(7)	0.2474(7)	0.2473(7)	
B _{eq}	0.51(1)	0.52(11)	0.40(9)	0.45(10)	

Notes: B_{eq} is an isotropic temperature factor. The numbers in parentheses denote errors in the last decimal place.

respectively. The unit-cell volume compressions of V/V₀ of the three samples are shown in Figure 1.

Bond distance

ABO₃ ilmenite structure is composed of AO₆ and BO₆ octahedra with shared faces. A and B cations across the shared face are alternatively located along c. On the other hand, the AO₆ and BO₆ octahedra are respectively located in a plane parallel to (001) and linked to adjacent octahedra via a shared edge. The configuration of two AO₆ and BO₆ octahedra is shown in Figure 2. The A-O and B-O bond distances, O-O octahedral edges, selected bond angles, and AO₆ and BO₆ volumes are presented as a function of pressure in Table 3. All the oxygen atoms (O1 to O9, indicated in Fig. 2) occupy crystallographically equivalent positions. These octahedra have a pair of three equivalent bond distances, M-O (sh face) and M-O (unsh face) (M: A and B). M-O (sh face) and M-O (unsh face) bond lengths are presented as a function of pressure in Figure 3. Bond angle ∠O-M-O (sh face) corresponds to the O1-O2-O3 shared face and ∠O-M-O (unsh face) to the O4-O5-O6 face for AO₆ and the O7-O8-O9

TABLE 3A. Interatomic distances, bond angles, and octahedral volumes

MgSiO ₃					
Press (GPa)	0.0001	3.5	5.7	7.8	
MgO ₆					
Mg-O1 (sh face) ×3	2.186(1)	2.158(3)	2.136(6)	2.129(9)	
Mg-O4 (unsh face) ×3	1.992(1)	1.985(4)	1.986(7)	1.981(6)	
<Mg-O>	2.089	2.072	2.061	2.055	
O1-O4 (sh edge) ×3	2.965(1)	2.936(4)	2.920(9)	2.892(9)	
O1-O6 (unsh edge) ×3	3.082(1)	3.053(4)	3.035(9)	3.027(10)	
O1-O2 (sh face) ×3	2.509(1)	2.499(4)	2.488(9)	2.500(11)	
O4-O6 (unsh face) ×3	3.073(1)	3.057(4)	3.054(6)	3.048(7)	
∠O4-Mg-O6 (unsh face)	100.96(4)	100.74(9)	100.5(2)	100.6(3)	
∠O1-Mg-O2 (sh face)	70.06(5)	70.77(1)	71.3(3)	72.1(4)	
V(MgO ₆) (Å ³)	11.42(2)	11.18(4)	11.04(9)	10.98(10)	
SiO ₆					
Si-O1 (sh face)	1.825(1)	1.823(3)	1.816(6)	1.828(9)	
Si-O7 (unsh face)	1.756(1)	1.748(2)	1.747(5)	1.732(6)	
<Si-O>	1.790	1.786	1.781	1.779	
O3-O9 (sh edge) ×3	2.304(1)	2.304(3)	2.298(9)	2.300(9)	
O3-O8 (unsh edge) ×3	2.657(2)	2.652(3)	2.647(9)	2.649(9)	
O1-O3 (sh face) ×3	2.509(2)	2.500(3)	2.489(6)	2.507(6)	
O8-O9 (unsh face) ×3	2.644(1)	2.631(4)	2.629(9)	2.600(9)	
∠O8-Si-O9 (unsh face)	97.69(5)	97.64(9)	97.6(2)	97.3(3)	
∠O1-Si-O3 (sh face)	86.84(5)	86.54(9)	86.5(2)	86.6(4)	
V(SiO ₆) (Å ³)	7.480(1)	7.42(3)	7.36(8)	7.35(8)	
Mg1-Si1	2.7465(12)	2.718(3)	2.698(9)	2.680(8)	
Mg1-Mg2	2.8265(7)	2.806(1)	2.793(2)	2.785(2)	
Si1-Si2	2.7410(6)	2.729(1)	2.723(1)	2.718(1)	
Void space (Å ³)					
Void/cell	149.2	146.9	145.7	144.1	
λ (MgO ₆)	1.044(1)	1.041(1)	1.039(3)	1.037(3)	
σ ² (MgO ₆) (°)	143.0(1)	138.0(3)	133.0(7)	125.0(7)	
λ (SiO ₆)	1.015(1)	1.015(1)	1.015(3)	1.015(4)	
σ ² (SiO ₆) (°)	54.6(7)	52.0(1)	54.0(5)	52.0(5)	

Notes: Atom names are specified in Figure 3. Abbreviations sh and unsh are shared and unshared bond or face, respectively.

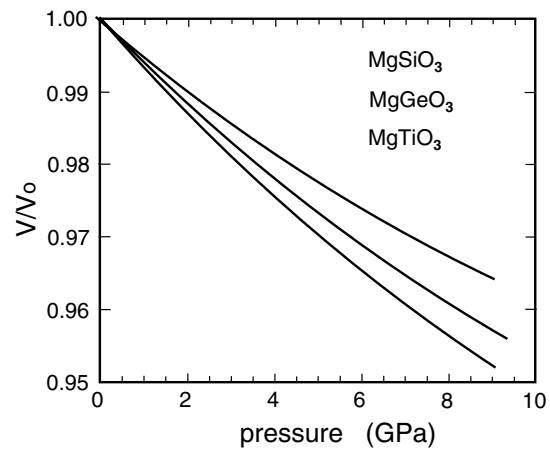


FIGURE 1. Unit-cell volume compression of MgSiO₃, MgGeO₃, and MgTiO₃ with increasing pressure. Solid lines are shown for the bulk modulus of MgSiO₃ reported by Weidner and Ito (1985), MgGeO₃ by Sato and Akimoto (1977), and MgTiO₃ by Liebermann (1976).

face for BO₆ opposite the vacant space.

The longer M-O (sh face) bonds are more shortened under pressure than shorter M-O (unsh face) bonds. Therefore, the cation shifts toward the center of the octahedron. Compressions of B-O (B = Si, Ge, Ti) bond lengths are smaller than those of A-O (A = Mg). The shared edge of the octahedron, O-O (sh edge),

TABLE 3B. —Continued

MgGeO ₃	0.0001	1.8	4.7	8.1	9.3
Press (GPa)					
MgO ₆					
Mg-O1 (sh)	2.185 (4)	2.176 (7)	2.161(12)	2.146(17)	2.128(8)
Mg-O4 (unsh)	2.024 (3)	2.013 (6)	2.004(10)	1.987(12)	1.983(6)
<Mg-O>	2.104	2.094	2.083	2.067	2.055
O1-O4 (sh edge) ×3	2.956 (4)	2.939 (9)	2.923(14)	2.888(19)	2.882(10)
O1-O6 (unsh edge) ×3	3.019 (4)	2.999 (9)	2.978(14)	2.950(19)	2.926(10)
O1-O2 (sh face) ×3	2.602 (6)	2.596 (6)	2.585(12)	2.587(12)	2.567(5)
O4-O6 (unsh face) ×3	3.156 (4)	3.143 (4)	3.129(7)	3.104(7)	3.095(4)
∠O4-Mg-O6 (unsh face)	102.5(2)	102.7(2)	102.6(4)	102.7(6)	102.6(3)
∠O1-Mg-O2 (sh face)	73.1 (1)	73.2 (3)	73.4(5)	74.1(7)	74.2(3)
V (MgO ₆) (Å ³)	11.80 (5)	11.63 (8)	11.45(13)	11.21(2)	11.04(8)
GeO ₆					
Ge-O1 (sh face)	1.946 (6)	1.944 (5)	1.934(9)	1.934(13)	1.930(6)
Ge-O7 (unsh face)	1.851 (5)	1.847 (5)	1.844(7)	1.831(9)	1.833(4)
<Ge-O>	1.898	1.895	1.889	1.882	1.881
O3-O9 (sh edge) ×3	2.484 (4)	2.484 (9)	2.476(14)	2.473(19)	2.475(10)
O3-O8 (unsh edge) ×3	2.822 (5)	2.816 (5)	2.812(9)	2.787(10)	2.801(4)
O1-O3 (sh face) ×3	2.601 (4)	2.596 (4)	2.585(7)	2.587(7)	2.567(3)
O8-O9 (unsh face) ×3	2.791 (4)	2.786 (8)	2.774(13)	2.762(18)	2.761(9)
∠O8-Ge-O9 (unsh face)	99.4 (3)	99.4 (2)	99.3(3)	99.1(4)	99.6(2)
∠O1-Ge-O3 (sh face)	83.9 (3)	83.7 (2)	83.9(4)	83.9(5)	83.2(2)
V (GeO ₆) (Å ³)	8.90 (4)	8.86 (7)	8.77(11)	8.69(14)	8.66(7)
Mg1-Ge1	2.8229 (9)	2.817 (2)	2.792(2)	2.771(1)	2.766(8)
Mg1-Mg2	2.936 (1)	2.929 (1)	2.916(2)	2.900(3)	2.890(2)
Ge1-Ge2	2.8731 (4)	2.865 (1)	2.855(1)	2.840(1)	2.8369(6)
Void space (Å ³)	165.9	164.3	162.3	159.1	159.3
Void / cell	0.5718	0.5719	0.5722	0.5713	0.5725
λ (MgO ₆)	1.036(1)	1.036(1)	1.035(3)	1.034(3)	1.033(6)
σ ² (MgO ₆) (°)	121.0(1)	120.0(3)	118.0(7)	114.0(7)	112.0(4)
λ (GeO ₆)	1.017(1)	1.017(1)	1.016(3)	1.016(4)	1.017(2)
σ ² (GeO ₆) (°)	58.0(2)	57.0(3)	57.0(5)	54.0(5)	58.0(3)

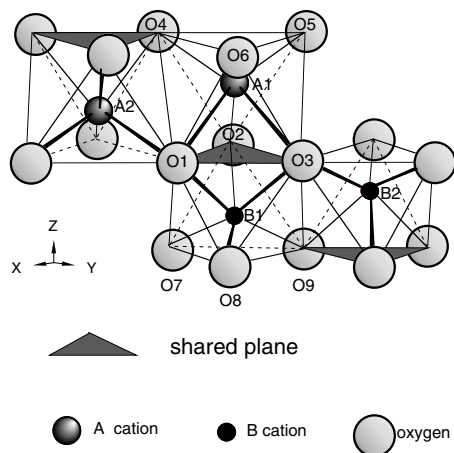


FIGURE 2. Linkage of AO₆ and BO₆ octahedra. Each cation and anion has a crystallographically equivalent position but is assigned an individual name for the sake of discussion.

changes less with pressure than the O-O (unsh edge).

In all three ilmenites, MgSiO₃, MgGeO₃, and MgTiO₃, the three M-O (sh face) bonds are longer than those of M-O (unsh face). This is because the A-B repulsion makes the former bonds more elongated than the latter. With increasing pressure M-O (sh face) of both octahedra of these samples is more compressive

TABLE 3C. —Continued

MgTiO ₃	0.0001	3.1	5.8	8.1
Press (GPa)				
MgO ₆				
Mg-O1 (sh face)	2.1655(9)	2.149(12)	2.129(15)	2.122(12)
Mg-O4 (unsh face)	2.0480(8)	2.028(9)	2.022(11)	2.007(9)
<Mg-O>	2.1067	2.089	2.076	2.065
O1-O4 (sh edge) ×3	2.9442(9)	2.902(12)	2.884(19)	2.876(12)
O1-O6 (unsh edge) ×3	2.9781(9)	2.941(12)	2.917(19)	2.895(12)
O1-O2 (sh plane) ×3	2.6750(6)	2.667(12)	2.642(11)	2.636(10)
O4-O6 (unsh face) ×3	3.1878(7)	3.171(7)	3.164(7)	3.140(6)
∠O4-Mg-O6 (unsh face)	102.21(9)	102.8(4)	102.9(5)	102.9(4)
∠O1-Mg-O2 (sh face)	76.31(7)	76.7(5)	76.7(6)	76.7(5)
V (MgO ₆) (Å ³)	11.99(1)	11.67(10)	11.45(20)	11.27(11)
TiO ₆				
Ti-O1 (sh face)	2.0912(7)	2.091(9)	2.069(14)	2.066(9)
Ti-O7 (unsh face)	1.8658(5)	1.856(7)	1.855(9)	1.851(7)
<Ti-O>	1.9785	1.974	1.962	1.959
O3-O9 (sh edge) ×3	2.6134(9)	2.616(13)	2.598(21)	2.593(13)
O3-O8 (unsh edge) ×3	2.8810(9)	2.881(13)	2.868(19)	2.846(11)
O1-O3 (sh face) ×3	2.6750(7)	2.667(7)	2.642(11)	2.636(6)
O8-O9 (unsh face) ×3	2.9140(7)	2.894(9)	2.889(9)	2.893(9)
∠O8-Ti-O9 (unsh face)	102.69(3)	102.4(3)	102.3(5)	102.8(3)
∠O1-Ti-O3 (sh face)	79.52(3)	79.2(4)	79.4(6)	79.3(4)
V (TiO ₆) (Å ³)	9.926(9)	9.86(11)	9.69(15)	9.62(10)
Mg1-Ti1	2.9318(4)	2.914(10)	2.884(14)	2.879(14)
Mg1-Mg2	2.9854(4)	2.970(3)	2.956(3)	2.947(4)
Ti1-Ti2	2.9809(3)	2.965(2)	2.949(2)	2.944(2)
Void space (Å ³)	172.9	170.6	173.0	168.4
Void / cell	0.5722	0.5720	0.5731	0.5732
λ (MgO ₆)	1.027(1)	1.028(1)	1.028(11)	1.027(10)
σ ² (MgO ₆) (°)	92.0(1)	94.0(3)	95.0(7)	90.0(7)
λ (SiO ₆)	1.030(1)	1.029(1)	1.029(3)	1.029(4)
σ ² (SiO ₆) (°)	54.0(7)	52.0(3)	54.0(5)	52.0(5)

than M-O (unsh face). AO₆ exhibits a more obvious tendency than BO₆. MgSiO₃ has the smallest compressibilities of M-O (sh face) and M-O (unsh face) among the ilmenites.

AO₆ and BO₆ octahedra

The unit cells of ilmenites are composed of AO₆ and BO₆ octahedra and void space. These octahedral volumes are not equally compressed with pressure. The volume changes of MgSiO₃, MgGeO₃, and MgTiO₃ with pressure are in good agreement with the data recalculated from the previously reported bulk moduli of MgSiO₃ observed by Brillouin scattering (Weidner and Ito 1985), of MgGeO₃ by powder diffraction (Sato and Akimoto 1977), and of MgTiO₃ by ultrasonic measurement (Liebermann 1976). Table 4 presents the bulk moduli of the unit cell, AO₆, and BO₆. The data for FeTiO₃ (Wechsler and Prewitt 1984) and MnGeO₃ (Ross et al. 1993) are also presented in Table 4. The bulk moduli of MgSiO₃, MgGeO₃, and MgTiO₃ as a function of B-cation radii are plotted in Figure 4. The moduli change linearly with the radii.

The larger AO₆ (MgO₆) octahedron is more compressed than the smaller BO₆ (SiO₆, GeO₆, and TiO₆) octahedron, as seen in Figure 5. Therefore, the volume ratio of BO₆/AO₆ changes toward 1.0 with increasing pressure. The volumes of AO₆ and BO₆ in MgTiO₃ become very similar to each other but those in MgSiO₃ continue to have very different volumes, even at high pressure.

The bulk moduli of BO₆ for all five samples are much larger than those of AO₆. MgO₆ and SiO₆ in MgSiO₃ are the most rigid AO₆ and BO₆ octahedra of all five samples. Note that MgSiO₃ is stable at high-pressure and can be synthesized over 20 GPa.

TABLE 4. Bulk modulus (GPa) of the unit cell and of the AO₆ and BO₆ octahedra

		Unit cell	AO ₆	BO ₆	Method
MgSiO ₃	(this study)	219(4)	172(7)	292(6)	single crystal
	(Weider and Ito 1985)	212			Brillouin scattering
MgGeO ₃	(this study)	180(9)	139(3)	268(4)	single crystal
	(Sato et al. 1977)	187(2)			powder diffraction
MgTiO ₃	(this study)	161(1)	116(1)	245(19)	single crystal
	(Liebermann, 1976)	169			ultra sonic
FeTiO ₃	(Wechsler and Prewitt 1984)	177(3)	131(6)	267(15)	single crystal
MnGeO ₃	(Ross et al. 1993)	173(4)	131(1)	208(36)	single crystal

Note: All moduli of K_0 observed in the present study are calculated from $K_0' = 4$ in the Birch-Murnaghan equation of state.

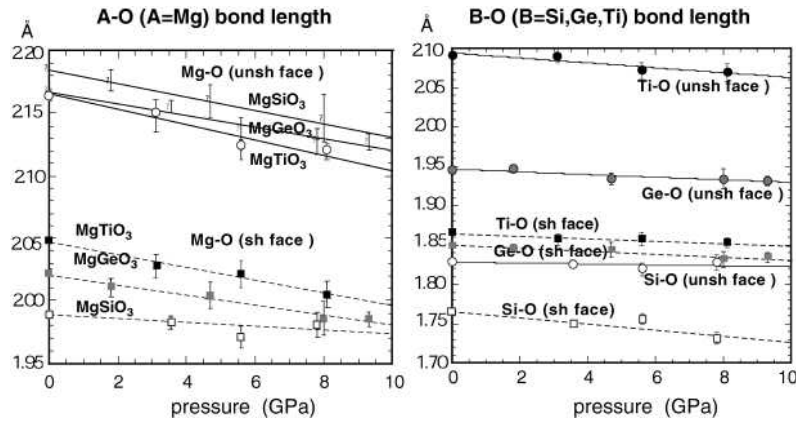


FIGURE 3. A-O (A = Mg) and B-O (B = Si, Ge, Ti) bond length. The abbreviation sh represents M-O bonds with oxygen atoms composing shared faces and the abbreviation unsh represents bonds with oxygen atoms opposite to the shared face. Dashed lines represent the former distances and solid lines indicate the latter distances.

Site occupancy

Lattice compression may have an effect on the site occupancies. A site-occupancy test was undertaken in the present structure refinement and proved the ordered distribution of A and B cations within the experimental region. Since the present experiment was executed at ambient temperature, cation exchange between the two sites did not happen. This is also shown by the isotropic thermal parameter B_{iso} , which is partly related to the positional disorder of the cation. This term becomes linearly smaller with increasing pressure. The cation ordering at two sites should be controlled by sample preparation at high temperature and pressure. Thermal energy is probably more effective than pressure for atomic thermal vibration inducing cation exchange.

Deformation of AO₆ and BO₆ octahedra

Since each octahedron has a shared face and three shared edges, octahedral compression leads to an inhomogeneous deformation. The quadratic elongation (λ) and bond angle variance (σ^2) (Robinson et al. 1971) were applied to comprehend the polyhedral distortion and finite homogeneous strain. These two terms, σ^2 and λ (Table 3), suggest an anisotropic compression of AO₆ and BO₆. λ for each sample becomes gradually smaller toward $\lambda = 1.0$ with increasing pressure and σ^2 also decreases with pressure. λ for MgSiO₃, MgGeO₃, MgTiO₃, FeTiO₃, and MnGeO₃ is plotted as a function of $V(\text{BO}_6)/V(\text{AO}_6)$ in Figure 6. In the case of a large difference in the volumes between AO₆ and BO₆, λ of AO₆ is large under ambient conditions and becomes smaller as pressure increases, which indicates that the regularity of the octahedron is enhanced at higher pressure. Both σ^2 and λ verify the reduction of the deformation of AO₆ and BO₆

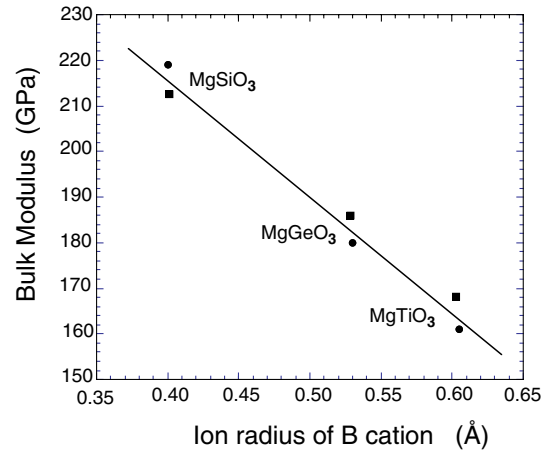


FIGURE 4. Bulk modulus of MgSiO₃, MgGeO₃, and MgTiO₃ as a function of B cation radius.

octahedra. MgTiO₃ and FeTiO₃ have almost the same λ values for their AO₆ and BO₆ octahedra. The corundum-type structures of Al₂O₃, Fe₂O₃, Cr₂O₃, and V₂O₃ have the same A and B cations and their λ values are in the range 1.01–1.03.

In the ideal case the cation is located at the center of the octahedron, but in ilmenite, corundum, and LiNbO₃ the cation shifts in the c direction away from the center, as seen in Figure 2. This deviation leads to polarization or a dipole moment, which causes dielectricity in the LiNbO₃ structure. The cation position moves with pressure, as indicated by the difference in z between the oxygen atoms and the cations (Table 5). Mg and Si in MgSiO₃ ilmenite tends to approach the center of MgO₆ and SiO₆ with increasing pressure. The positional deviation of cations in MgGeO₃

and MgTiO₃ is not so remarkable in comparison with MgSiO₃. However, they also show the same tendency with pressure.

DISCUSSION

The ilmenite structure has both shared-face and shared-edge configurations of AO₆ and BO₆ octahedra. The A-B cations are located across the shared face and A-A and B-B across the shared edge. The A-B interatomic distance along *c* becomes shorter and more compressed than A-A and B-B with increasing pressure. Accordingly, *c* is more compressive than *a* and *c/a* becomes smaller with increasing pressure. Consequently, the A-B interaction becomes more essential for their physical properties in comparison with the A-A and B-B interactions.

In corundum-type structures having the same A and B cations, the compression of the M-M interatomic distance can be discussed without consideration of ionic size difference. The M-M distance across the shared face in these structures is shorter than the M-M distance across the shared edge. The Al-Al distance across the shared face in Al₂O₃ is less compressible than that

across the shared edge, which is observed from structure analysis at high pressures up to 31 GPa (Kim-Zajonz et al. 1999). The comparative effect of these compressions is different from the present ilmenite studies. Naturally the *c/a* variation with pressure is different between the ilmenite and corundum structures.

Hazen and Prewitt (1977) discussed the effects of temperature and pressure on interatomic distances in oxide minerals. They proposed an almost linear compression of M-O distances. In the present experiment, the mean Mg-O distance shows a large (different) compression in all three samples (Table 3) in spite of same bond strength, coordination, and formal charge of their structures. The difference in M-O is caused by ionic size effect, configuration, and electron negativity difference between the A and B cations and probably the reduced mass of these cations as well.

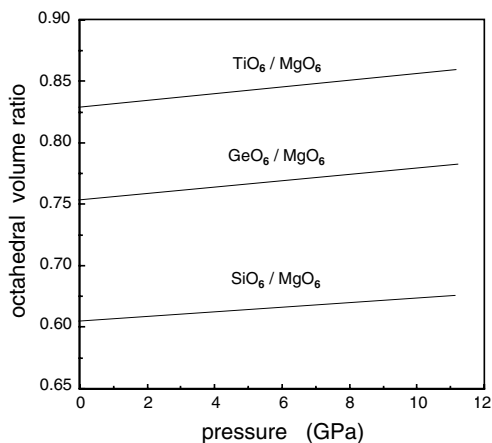


FIGURE 5. Octahedral volume ratio $V(\text{BO}_6)/V(\text{AO}_6)$ as a function of pressure.

TABLE 5. Cation deviation along the *c* axis from the center of AO₆ and BO₆ octahedra

MgSiO ₃	Press (GPa)	0.0001	3.5	5.7	7.8	
<i>z</i> (Mg)- <i>z</i> (Ou)		0.0668	0.067	0.0682	0.0682	
<i>z</i> (Mg)- <i>z</i> (Os)		0.1207	0.1188	0.1179	0.1169	
deviation		1.807	1.773	1.729	1.714	
<i>z</i> (Si)- <i>z</i> (Ou)		0.0600	0.0645	0.0645	0.0650	
<i>z</i> (Si)- <i>z</i> (Os)		0.0819	0.0830	0.0828	0.0836	
deviation		1.365	1.287	1.284	1.286	
MgGeO ₃	Press (GPa)	0.0001	1.8	4.7	8.1	9.3
<i>z</i> (Mg)- <i>z</i> (Ou)		0.0641	0.0634	0.0638	0.0635	0.0639
<i>z</i> (Mg)- <i>z</i> (Os)		0.1154	0.1151	0.1149	0.1142	0.1134
deviation		1.800	1.815	1.801	1.798	1.775
<i>z</i> (Ge)- <i>z</i> (Ou)		0.0639	0.0642	0.0643	0.0647	0.0642
<i>z</i> (Ge)- <i>z</i> (Os)		0.0899	0.0907	0.0904	0.0910	0.0919
deviation		1.407	1.413	1.406	1.407	1.431
MgTiO ₃	Press (GPa)	0.0001	3.1	5.8	8.1	
<i>z</i> (Mg)- <i>z</i> (Ou)		0.0646	0.0634	0.0630	0.0634	
<i>z</i> (Mg)- <i>z</i> (Os)		0.1092	0.1087	0.1081	0.1087	
deviation		1.6904	1.714	1.715	1.715	
<i>z</i> (Ti)- <i>z</i> (Ou)		0.0580	0.0581	0.0598	0.0586	
<i>z</i> (Ti)- <i>z</i> (Os)		0.1015	0.1026	0.1025	0.1027	
deviation		1.750	1.766	1.714	1.753	

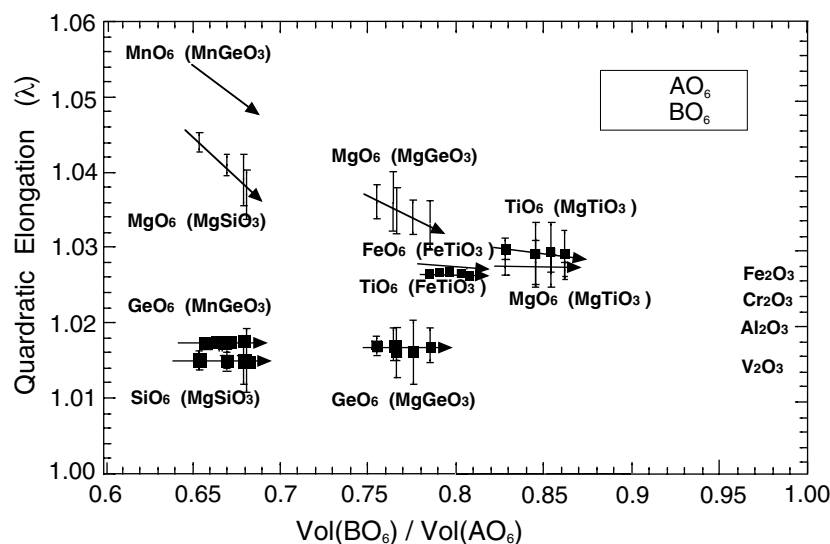


FIGURE 6. Quadratic elongation (λ) of AO₆ and BO₆ octahedra against their volume ratios $V(\text{BO}_6)/V(\text{AO}_6)$. Data related to MnGeO₃ and FeTiO₃ were obtained by recalculation from Ross et al. (1993) and Wechsler and Prewitt (1984). The double circle indicates data for corundum structures. The data for Fe₂O₃, Cr₂O₃, and V₂O₃ were calculated from Finger and Hazen (1980).

The polyhedral volume and its compressibility are reflected by the size of the adjacent polyhedra and void spaces and by the configuration of the polyhedra. In the case where the volume of both octahedra become almost equivalent at high pressure, the replacement between A and B cations can be possible, resulting in a cation-disordered arrangement. An alternative replacement in ilmenite induces the LiNbO₃-type structure. A random replacement or highly disordered exchange brings about the corundum structure. However, there has been no report of the phase transition from ilmenite directly to LiNbO₃- or corundum-type structures.

It has been reported that MgTiO₃, FeTiO₃, MnSnO₃, ZnGeO₃, and MgGeO₃ ilmenites have LiNbO₃ polymorphs as metastable phases with release of pressure from the perovskite state (Leinenweber et al. 1991). Their recovered LiNbO₃ polymorphs have a somewhat denser structure than the corresponding ilmenite structure (Ko and Prewitt 1988; Leinenweber et al. 1991). The smaller density can be explained by the cation order. The array of alternating A-B cations in a row along **a** in the LiNbO₃ type structure gives a shorter cell edge than that of the ilmenite structure with A-A and B-B in two different rows.

Crystal chemical systematics among ilmenite, LiNbO₃, and perovskite structures were discussed by Navrotsky (1998). However, neither clear evidence nor discussion for the metastable phase of the LiNbO₃-type structure at high pressure has been found. The LiNbO₃ polymorph has a smaller volume than the ilmenite phase, indicating $\Delta V < 0$ at the transition from ilmenite to LiNbO₃ and the alternative ordering of A and B cations in LiNbO₃, resulting in $\Delta S > 0$. Hence the LiNbO₃-type polymorph is possibly stable at high pressure. Lipton et al. (1999) determined the enthalpy of transformation of MgTiO₃ from ilmenite to the LiNbO₃-type structure. The latter structure is more stable at higher pressure. Hence ilmenite may transform to the LiNbO₃-type structure under the condition of adequate mobility by heating at high pressure.

The present high-pressure diffraction studies were conducted at ambient temperature and we could not find phase transition either to perovskite or to the LiNbO₃ phase within the experimental pressure range. A phase transformation to LiNbO₃ due to compression alone is unlikely, even if further compression is applied. Thermal energy may be needed for the cation replacement. However, MgSiO₃ and MnTiO₃ with large differences in cation size cannot expect the LiNbO₃ structure. They revert to the ilmenite structure from the perovskite structure during the release of pressure.

REFERENCES CITED

- Deer, W. A. and Zussman, J., Eds. (1963) *Rock Forming Minerals*, 5, 30–32. Longmans, Green and Co. Ltd., London.
- Finger, L.W. and Hazen, R.M. (1980) Crystal structure and isothermal compression of Fe₂O₃, Cr₂O₃ and V₂O₅ to 50 kbars. *Journal of Applied Physics*, 51, 5362–5367.
- Hazen, R.M. and Prewitt, C.T. (1977) Effects of temperature and pressure on interatomic distance in oxygen-based minerals. *American Mineralogist*, 62, 309–315.
- Horiuchi, H., Hirano, M., Ito, E., and Matsui, Y. (1982) MgSiO₃ (ilmenite-type): single crystal X-ray diffraction study. *American Mineralogist*, 67, 788–793.
- Ito, E. and Navrotsky, A. (1985) MgSiO₃ ilmenite: Calorimetry, phase equilibria and decomposition at atmospheric pressure. *American Mineralogist*, 70, 1020–1026.
- Ito, E. and Yamada, H. (1982) Stability relations of silicate spinels, ilmenites and perovskites. In S. Akimoto and M.H. Manghni, Eds., *High Pressure Research in Geophysics*, 405–419. Center of Academic Publications, Tokyo.
- Karki, B., Duan, W., da Silva, C.R.S., and Wentzcovitch, R.M. (2000) Ab initio structure of MgSiO₃ ilmenite at high pressure. *American Mineralogist*, 85, 317–320.
- Kim-Zajonz, J., Werner, S., and Shultz, H. (1999) High pressure single crystal X-ray diffraction study on ruby up to 31GPa. *Zeitschrift für Kristallographie*, 214, 331–336.
- Ko, J. and Prewitt, C.T. (1988) High-pressure phase transition in MnTiO₃ from the ilmenite to the LiNbO₃ structure. *Physics and Chemistry of Minerals*, 15, 355–362.
- Leinenweber, K., Utsumi, W., Tsuchida, Y., Yagi, T., and Kurita, K. (1991) Unquenchable high-pressure perovskite polymorphs of MnSnO₃ and FeTiO₃. *Physics and Chemistry of Minerals*, 18, 244–250.
- Leinenweber, K., Wang, Y., Yagi, T., and Yusa, H. (1994) Quenchable perovskite phase of MgGeO₃ and comparison with MgSiO₃ perovskite. *American Mineralogist*, 79, 197–199.
- Liebermann, R.C. (1976) Elasticity of ilmenites. *Physics of the Earth and Planetary Interiors*, 12, 5–10.
- Lipton, J.A., Fei, Y., and Navrotsky, A. (1997) Complete Fe-Mg solid solution in lithium niobate and perovskite structures in titanates at high pressures and temperatures. *American Mineralogist*, 82, 639–642.
- (1999) The MgTiO₃-FeTiO₃ join at high pressure and temperature. *American Mineralogist*, 84, 1595–1603.
- Matsui, M., Akaogi, M., and Matsumoto, T. (1987) Computational model of the structural and elastic properties of the ilmenite and perovskite phase of MgSiO₃. *Physics and Chemistry of Minerals*, 14, 101–106.
- Mukaïda, T., Yagi, T., Niyajima, N., Kondo, T., Sata, N., and Kikegawa, T. (2003) High-pressure and high-temperature phase transformations in KlnbO₃. *Journal of Applied Physics*, 93, 3852–3858.
- Navrotsky, A. (1998) Energetics and crystal chemical systematics among ilmenite, lithium niobate and perovskite structures. *Chemistry of Materials*, 10, 2787–2793.
- Reynard, B. and Rubie, D.C. (1996) High-pressure, high-temperature Raman spectroscopic study of ilmenite type MgSiO₃. *American Mineralogist*, 81, 1092–1096.
- Reynard, B., Fiquet, G., Itie, J.P., and Rubie, D.C. (1996) High-pressure X-ray diffraction study and equation of state of MgSiO₃ ilmenite. *American Mineralogist*, 81, 45–50.
- Robinson, K., Gibbs, G.V., and Ribbe, P.H. (1971) Quadratic elongation: A quantitative measure of distortion in coordination polyhedra. *Science*, 172, 567–570.
- Ross, N.L. and Leinenweber, K. (1990) Single crystal structure refinement of high-pressure ZnGeO₃ ilmenite. *Zeitschrift für Kristallographie*, 191, 93–104.
- Ross, N.L. and Navrotsky, A. (1988) Study of the MgGeO₃ polymorphs (orthopyroxene, clinopyroxene and ilmenite structures) by calorimetry, spectroscopy and phase equilibria. *American Mineralogist*, 97, 1355–1365.
- Ross, N.L., Ko, J., and Prewitt, C.T. (1989) A new phase transition in MnTiO₃: LiNbO₃-perovskite structure. *Physics and Chemistry of Minerals*, 16, 621–629.
- Ross, N.L., Reynard, B., and Guyot, F. (1993) High-pressure structural study of MnGeO₃ ilmenite. *Zeitschrift für Kristallographie*, 204, 43–55.
- Sasaki, S. (1987) A Fortran program for the least-squares refinement of crystal structures. National Laboratory for High Energy Physics, Japan.
- Sato, Y., Ito, E., and Akimoto, S. (1977) Hydrostatic compression of ilmenite phase of ZnSiO₃ and MgGeO₃. *Physics and Chemistry of Minerals*, 2, 171–176.
- Sawamoto, H. (1987) Phase diagram of MgSiO₃ at pressure up to 24 GPa and temperatures up to 2200 °C: Phase stability and properties of tetragonal garnet. In M.H. Manghni and Y. Syono, Eds., *High-Pressure Research in Mineral Physics*, 209–219. American Geophysical Union, Washington, D.C.
- Tomioka, N. and Fujino, K. (1997) Natural (Mg,Fe)SiO₃-ilmenite and perovskite in the Tenham meteorite. *Science*, 277, 352–355.
- Wechsler, B.A. and Prewitt, C.T. (1984) Crystal structure of ilmenite (FeTiO₃) at high temperature and at high pressure. *American Mineralogist*, 69, 176–185.
- Weidner, D.J. and Ito, E. (1985) Elasticity of MgSiO₃ in the ilmenite phase. *Physics of Earth and Planetary Interiors*, 40, 65–70.
- Yamanaka, T., Fukuda, T., Hattori, T., and Sumiya, H. (2001) New diamond anvil cell for single crystal analysis. *Review of Science Instruments*, 72, 1458–1462.
- Yamanaka, T., Fukuda, T., and Mimaki, J. (2002) Bonding character of SiO₂ stishovite under high pressures up to 30 GPa. *Physics and Chemistry of Minerals*, 29, 633–641.

MANUSCRIPT RECEIVED FEBRUARY 9, 2004

MANUSCRIPT ACCEPTED DECEMBER 22, 2004

MANUSCRIPT HANDLED BY YINGWEI FEI